NANO LETTERS

Letter

pubs.acs.org/NanoLett

# High Brightness InP Micropillars Grown on Silicon with Fermi Level Splitting Larger than 1 eV

Thai-Truong D. Tran,[†] Hao Sun,[‡,†] Kar Wei Ng,[†] Fan Ren,[†] Kun Li,[†] Fanglu Lu,[†] Eli Yablonovitch,[†] and Constance J. Chang-Hasnain*[,†]

[†]Applied Science and Technology Group and Department of Electrical Engineering and Computer Sciences, University of California at Berkeley, Berkeley, California 94720, United States

[‡]Department of Electronic Engineering, Tsinghua University, Beijing 100084, P. R. China

Supporting Information

**ABSTRACT:** The growth of III−V nanowires on silicon is a promising approach for low-cost, large-scale III−V photovoltaics. However, performances of III−V nanowire solar cells have not yet been as good as their bulk counterparts, as nanostructured light absorbers are fundamentally challenged by enhanced minority carriers surface recombination rates. The resulting nonradiative losses lead to significant reductions in the external spontaneous emission quantum yield, which, in turn, manifest as penalties in the open-circuit voltage. In this work, calibrated photoluminescence measurements are utilized to construct equivalent voltage−current characteristics relating illumination intensities to Fermi level splitting $\Delta F$ inside InP microillars. Under 1 sun, we show that splitting can exceed $\Delta F \sim 0.90$ eV in undoped pillars. This value can be increased to values of $\Delta F \sim 0.95$ eV by cleaning pillar surfaces in acidic etchants. Pillars with nanotextured surfaces can yield splitting of $\Delta F \sim 0.90$ eV, even though they exhibit high densities of stacking faults. Finally, by introducing n-dopants, $\Delta F$ of 1.07 eV can be achieved due to a wider bandgap energy in n-doped wurzite InP, the higher brightness of doped materials, and the extraordinarily low surface recombination velocity of InP. This is the highest reported value for InP materials grown on a silicon substrate. These results provide further evidence that InP micropillars on silicon could be a promising material for low-cost, large-scale solar cells with high efficiency.

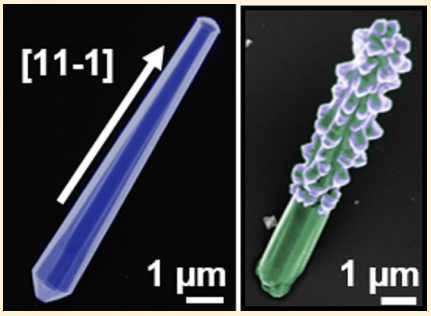


**KEYWORDS:** *Micropillars, nanowires, III−V on Si, photoluminescence, photovoltaics, solar cells*

The costs of photovoltaics (PV) need to be significantly reduced for PV to become competitive with other sources of energy. Increasing the energy conversion efficiency is a key strategy to decrease the costs of PV since both module and balance of systems costs have been shown to exhibit an inversely proportional relationship to the conversion efficiency.[1] Record energy conversion efficiencies are being attained with III−V semiconductors, but the high costs of III−V semiconductor substrates have prevented a widespread deployment of III−V based solar cells. One solution is to use epitaxial liftoff where the solar cell devices are removed from the native III−V substrates, which can subsequently be reused for growth.[2] The need for native III−V substrates could be avoided altogether by employing III−V nanowires, which can be synthesized on lower-cost, lattice-mismatched substrates such as silicon and could potentially combine the scalability of silicon technology with the efficiency of III−V materials.[3−6] However, even with single-crystalline material quality, the performances of III−V nanowire solar cells have so far been significantly inferior to those of planar, thin-film lifted-off III−V devices.[4−11]

The fundamental challenge of nanowire solar cells has been to obtain high open-circuit voltages ($V_{OC}$), as their large surface-to-volume ratios and the resulting nonradiative losses significantly reduce the external quantum yields for spontaneous emission, an important metric indicating reduced $V_{OC}$.[12,13] As the external quantum yield $\eta_{ext}$ is a very sensitive function of the internal quantum yield $\eta_i$,[13] even small reductions of $\eta_i$ due to material imperfections can result in sizable voltage penalties. $E_g - qV_{OC}$, where $E_g$ and $q$ denote the bandgap energy and elementary charge, respectively, is an important figure-of-merit in solar cells as it describes the loss of free energy per electron. There is an inverse relationship between the conversion efficiency and relative loss of free energy, $(E_g - qV_{OC})/E_g$, for published state-of-the-art solar cells made from different materials systems[14] (also see Table S1 in Supporting Information). To harness a solar cell's full potential, this loss has to be minimized. The open-circuit voltages in nanowire solar cells are often ∼0.7−1.0 V below the materials' bandgap,[11] which is especially penalizing for lower bandgap materials.

Recently, there has been progress in the performances of III−V nanowire solar cells.[5−10] While nanowire solar cells often

**Received:** February 17, 2014
**Revised:** May 6, 2014
**Published:** May 19, 2014

   dx.doi.org/10.1021/nl500621j | *Nano Lett.* 2014, 14, 3235−3240

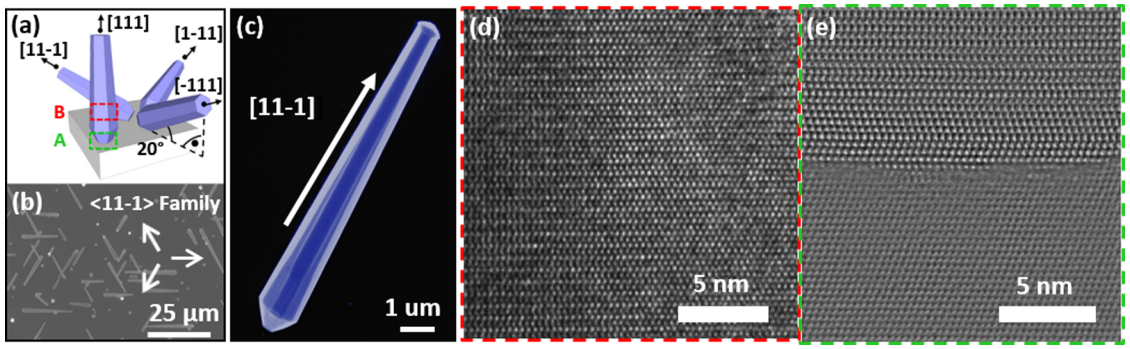


**Figure 1.** (a) Schematic of micropillars on (111) silicon substrate showing the possible growth directions. (b) Top view SEM of InP micropillars grown on (111)-Si. The InP micropillars are aligned upright (shown as bright white dots) or aligned in three other degenerate (111) directions as shown in (a). (c) Close-up image of as-grown InP micropillar. (d) HRTEM image showing the crystal lattice. Single crystalline, wurzite phase is observed with a characteristic zigzag arrangement. The image was taken at the main body of the pillar, which is completely free of defects (see box B in (a)). (e) HAADF image of the Si/InP interface. High-pass filtering is applied to remove the substantiate *z*-contrast between Si and InP. Roughness of the heterointerface comes from surface roughening of Si during sample preparation. InP seeds directly on silicon. Zinc blende–InP inclusion can be seen in this region of the pillar. The image was taken at the interface (see box A in (a)).

exhibit efficiencies of less than 5%,[11] recent progress has seen nanowire solar cells exceeding conversion efficiencies of 10%.[5,9,10] This is still significantly lower than the 28.8% and 22.1% conversion efficiencies achieved with planar GaAs and InP devices, respectively, grown on lattice-matched substrates.[14] The highest reported open-circuit voltage for nanowire solar cells was 0.906 V achieved with InP nanowires grown on an InP substrate.[9] The nanowires in those devices were a mixture of zinc blende and wurtzite InP. Since wurtzite InP exhibits a higher bandgap of 1.42 eV compared to the 1.34 eV zinc blende bandgap, a mean value of ~0.474 eV is estimated for the energy loss ($E_g - qV_{OC}$). It should be noted that low external quantum yields do not necessarily translate into low short-circuit currents, as long as carrier collection is adequate. Good short-circuit currents have been demonstrated with nanowire solar cells;[8,9,15−17] the fundamental challenge for nanostructured light absorbers is to achieve high open-circuit voltages.

In this study, we utilize photoluminescence (PL) techniques to measure Fermi level splitting in InP micropillars directly grown on silicon substrates. It has been shown that Fermi level splitting measured by such contactless techniques accurately matches conventional voltage–current ($V$–$I$) measurements using electrical contacts.[18−20] We found that Fermi level splitting under 1 sun illumination reaches 1.07 eV in doped pillars, the highest reported value for InP materials. This value is 0.46 eV below the material's absorption edge, which is similar compared to what has been achieved in the record planar InP solar cell.[14] This high splitting can be ascribed to the wider bandgap energy of n-doped wurzite InP crystals, the increased external quantum yield in doped materials, and the excellent surface properties of InP materials, which exhibit surface recombination velocities orders of maganitude lower compared to that of GaAs.[21]

The micropillars used in this experiment were grown catalyst-free at low temperatures of 450 °C with metal–organic vapor deposition (MOCVD) on (111) silicon substrates.[22] The InP micropillars are aligned to the family of ⟨111⟩ directions of the growth substrate, schematically illustrated in Figure 1a. Figure 1b, a top-view scanning electron micrograph (SEM), shows the nanopillars are aligned upright (shown as bright white dots) or aligned in three other degenerate (111) directions. Figure 1c shows a close-up SEM image of a typical as-grown InP micropillar with 1.3 $\mu$m diameter and 10.4 $\mu$m height. The growth conditions, precursors, and surface preparation were the same as those reported in ref 22. While the exact mechanism of the nucleation is still under current investigation, the subsequent core–shell growth is well understood.[23] Transmission electron microscopy studies (TEM) confirmed the single crystalline materials quality as well as the wurtzite crystal structure of the pillars, as shown in high-resolution TEM data in Figure 1d. Since the pillars grow in a core–shell growth mode, the pillar size can be scaled to such large diameters while preserving a defect free, single-cyrstalline wurtzite phase. Such large InP crystals with wurtzite phase are not obtained with thin film growth, as zinc blende is the thermodynamically favored crystal phase for large InP structures. The interface between the InP pillars and silicon substrate was studied, for the first time, at high magnification with high angle annular dark field (HAADF) imaging (see Figure 1e) InP has an 8% lattice mismatch with the silicon substrate. The misfit stress is relaxed via the formation of defects at the base of the pillar, as illustrated in Figure 1e. Instead of threading upward, these defects propagate laterally and terminate at the sidewall. The image in Figure 1e has been high-pass filtered to remove the very strong *z*-contrast between InP and Si; otherwise, the lattice on the silicon side cannot be identified clearly. The exact interface is not a straight line because silicon surface has been roughened by a TMAH etch during sample preparation to facilitate pillar nucleation. Stacking faults, i.e., zinc blende–InP inclusions, are clearly visible in this part of the pillar. The thickness/height of the interface part is approximately 200–400 nm, less than 5% of the total length. As a result of the characteristic core–shell growth, the stacking faults do not propagate into the pillars' main bodies, similar to what has been reported for InGaAs/GaAs nanopillars grown on silicon.[23]

As the surface-to-volume ratio scales with the diameter, the surface recombination rates in the micropillars are 5–10 times lower compared to those in nanowires whose diameters are often between 100 and 200 nm. Indeed, time-resolved photoluminescence (TRPL) measurements have shown that the carrier recombination lifetimes of pillars can be >7.4 ns at room temperature.[25] For comparison, lifetimes in III–V nanowires are often found to be of the order of 1–2 ns or considerably shorter.[26,27]


dx.doi.org/10.1021/nl500621j | *Nano Lett.* 2014, 14, 3235−3240

It is highly desirable to accelerate materials research by obtaining equivalent $V-I$ characteristics without having to fabricate devices with metal contacts. This is possible because the external luminescence of a material is proportional to $\exp[\Delta F/k_BT]$, where $k_BT$ denotes the thermal energy at room temperature. Calibrated PL measurements can yield Fermi level splitting $\Delta F$ of single, as-grown pillars, which, in turn, can be regarded as the maximum $V_{oc}$ achievable in that material. A monochromatic, continuous-wave (CW) laser with a wavelength of $\lambda$ = 660 nm was used with illumination intensities varied from 500 to 5 × $10^5$ W/m$^2$. An intensity of 600 W/m$^2$ corresponds to a photon flux density of 2 × $10^{17}$ photons/(s cm$^2$). This is the same flux density of all photons with energies greater than 1.42 eV for 1 sun irradiance (AM 1.5 condition). Hence, 600 W/m$^2$ of light with $\lambda$ = 660 nm is equivalent to 1 sun (AM 1.5) for InP pillars (1.42 eV bandgap energy). The collection efficiency of our experimental setup was calibrated with a near ideal reflector (see Supporting Information). Because of the well-known relationship between absorption and spontaneous emission, the Fermi level split $\Delta F$ inside a light absorber can be calculated from its total spontaneous emission rate:[18]

$$\Delta F = E + k_BT \ln\left(\frac{h^3c^2}{2\pi a E^2 A} r_{sp}\right) \quad (1)$$

Here, $E$ is the photon energy of spontaneous emission, $h$ the Planck constant, $c$ the speed of light in a vacuum, $A$ the surface area of the pillar, and $r_{sp}$ the total spontaneous emission rate emitted from the pillar per energy interval; $a$ denotes the absorptivity of the pillar for light which can be calculated to be $a \sim 1.5$ (see Supporting Information). Equation 1 can be derived from the van Roosbroeck–Shockley relationship, which results from the thermodynamic necessity that a light absorber at thermal equilibrium has to re-emit the same radiation that it absorbs.

The open-circuit voltage in a solar cell is a direct measurement of the difference in Fermi energy, i.e., the Fermi splitting, between the electrical contacts of anode and cathode. Therefore, the values for the Fermi level splitting are very good proxies for what voltages can be achieved with a material.

Figure 2 shows a photoluminescence spectrum of a single undoped, as-grown micropillar.[18] The emission spectrum shows

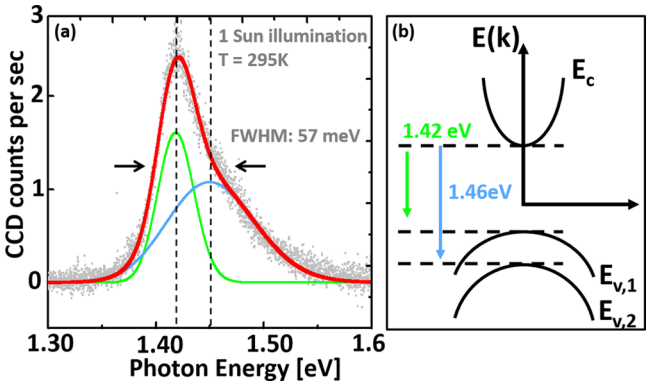


**Figure 2.** (a) PL spectrum from single pillar under illumination intensity equivalent to 1 sun. (b) Schematic depiction of the two transitions (at 1.42 and 1.46 eV) of wurtzite InP that are visible in the luminescence spectrum.

the two possible transitions of wurtzite InP at 1.42 and 1.46 eV,[24] significantly larger than the 1.34 eV bandgap energy of zinc blende crystalline-phase InP found in conventional, planar epitaxy (see Figure 2b). As will be shown, this is a contributing factor to a larger Fermi level splitting for the pillars. We estimate that the error of the values of the Fermi splitting is less than 2% (see Supporting Information).

The recombination current of photogenerated carriers inside a pillar can be modeled with[28]

$$I = AN + BN^2 + CN^3 \quad (2)$$

Equation 2 contains the $A$, $B$, and $C$ coefficients for Shockley–Read–Hall (SRH), radiative, and Auger recombination, respectively. In the high injection regime, i.e., the excess carrier density is large compared to the doping concentration of the material, the carrier density $N$ can be expressed as

$$N^2 = n_i^2 e^{\Delta F/k_BT} \quad (3a)$$

Here, $n_i$ denotes the intrinsic carrier density. In case of the low injection regime, i.e., the excess carrier densities are small compared to the doping concentration $N_D$, eq 3a becomes

$$N = \frac{n_i^2}{N_D} e^{\Delta F/k_BT} \quad (3b)$$

Using eq 3a (or eq 3b if it applies), and assuming that at a given Fermi level splitting one recombination mechanism dominates the others, one can rewrite eq 2 as

$$I \approx I_n e^{\Delta F/nk_BT} \quad (4)$$

In eq 4, the ideality factor $n$ depends on the dominant recombination mechanism. For radiative and Auger recombination, $n$ = 1 and $n$ = 2/3, respectively. For SRH recombination, at low injection levels, eq 3b applies and $n$ = 1, whereas for high illumination conditions, eq 3a applies and $n$ = 2. The proportionality constant $I_n$ depends on the dominant recombination mechanism. Taking the logarithm on both sides of eq 4, while considering that the recombination current $I$ is proportional to the illumination intensity $P$ and that there is a logarithmic relationship between Fermi level splitting $\Delta F$ and the spontaneous emission rate (see eq 1), one can rewrite eq 4 as

$$\ln(P) = \frac{\ln(r_{sp})}{n} + \text{const} \quad (5)$$

Equation 5 shows that illumination intensity $P$ versus spontaneous emission rate $r_{sp}$ is akin to a voltage–current ($V-I$) characteristic with the slope of the curve denoting the ideality factor, $n$.

Figure 3 shows such an equivalent $V-I$ characteristic obtained from a typical undoped, as-grown, single InP micropillar. (The characteristics of this particular pillar will be denoted with letter A.) The spontaneous emission rate and the Fermi level splitting are described by the bottom and top $x$-axes, while the illumination intensity is denoted by the $y$-axes. Measurements were performed at room temperature as well as 4 K. At 4 K the ideality factor $n \sim 1$ over the entire range of illumination intensities, suggesting that radiative recombination is the predominant mechanism and nonradiative recombination mechanisms are effectively suppressed. Hence, $\eta_i$ can be regarded to be near unity.[29] At room temperature (295 K) and low illumination levels, we found the ideality factor is still


dx.doi.org/10.1021/nl500621j | Nano Lett. 2014, 14, 3235–3240

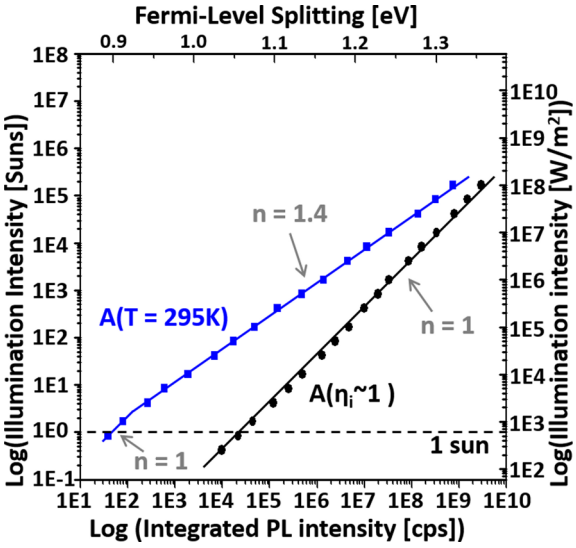


**Figure 3.** Equivalent $V$–$I$ curve of undoped InP micropillar A. The trace A($\eta_i \sim 1$) was obtained at cryogenic temperatures when the internal quantum yield is near unity. The bottom horizontal axis shows the integrated count rate; i.e., the count rates were integrated over the whole photoluminescence spectrum. For the calibration of the upper horizontal axis the spectral-density count rates were used, i.e., counts per second per energy interval.

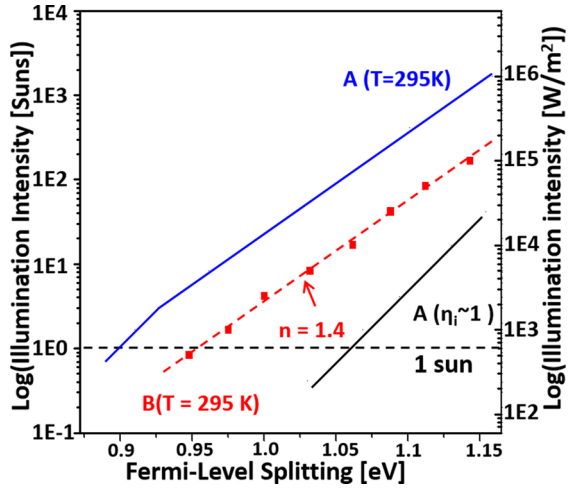


**Figure 4.** Equivalent $V$–$I$ characteristics of single, surface-treated InP micropillar (trace B). For comparison, the characteristics of the untreated, as-grown pillar shown in Figure 3 are also shown here (see traces A).

~1, while at higher illumination intensities, $n \sim 1.5$. This behavior of the ideality factor can be explained with SRH recombination as the illumination levels transition from the low to the high injection regime. At room temperature, $\eta_i$ can be determined by the ratio of PL intensities obtained at room temperature and 4 K. At 1 sun, an internal quantum yield of $\eta_i \sim 0.2\%$ is found. The Fermi level splitting reaches values larger than 0.90 eV under 1 sun, which is 0.52 eV below the material's bandgap.

Because of the large surface-to-volume ratio, the spontaneous emission quantum yield of pillars can be significantly improved by reducing the density of surface states positioned inside the materials bandgap. Such states could be due to oxygen atoms at the InP surface.[30] To thoroughly remove surface oxide, the pillars were first etched in a diluted piranha solution with $H_2SO_4$:$H_2O_2$:$H_2O$ (4:1:100) for 2 min and subsequently etched in a concentrated HCl:$H_2O$ (1:3) solution for 30 s.[31] Besides removing native oxide, it was reported that piranha solutions can remove carbon-related contaminations and defective material portions from InP nanowire surfaces, significantly improving solar cell performances.[10]

Figure 4 shows the equivalent $V$–$I$ curve obtained from such a surface treated pillar. At 1 sun illumination intensity the surface treated pillar is almost 1 order of magnitude brighter compared to untreated pillar, corresponding to Fermi level splitting of almost 0.95 eV. Here, the value for the voltage loss ($E_g - qV_{OC}$) is about 0.47 eV. While the results show that surface treatments are very effective, they have the disadvantage that the positive effects tend to last only for hours as the surfaces reoxidize.

An alternative to increase the external quantum yield of pillars is to increase radiative recombination rates of the material by doping and thereby increasing the $n{\cdot}p$ product inside the material. The radiative recombination rate can be expressed as[28]

$$r_{sp} = Bnp \tag{6a}$$

Here, $B$ denotes the radiative recombination coefficient and $n$ and $p$ describe the electron and hole densities. If the pillars are n-doped at levels considerably higher than the excess carrier density (low-level injection), then eq 6a becomes

$$r_{sp} = BN_D p \tag{6b}$$

To n-dope the pillars, diethyltellurium was flown into the MOCVD chamber during growth. Figure 5 compares the equivalent $V$–$I$ curve of a typical n-doped InP micropillar (trace B) with that of the undoped pillar discussed in Figure 3 (trace A). A more than 30× brighter luminescence is obtained for the doped micropillar at 1 sun illumination intensity. To estimate the doping concentration, we utilize the distinct shift of the photoluminescence peak due to the Burstein–Moss effect. Figure 5a shows that the photoluminescence peak of the doped InP pillars is shifted by 110 meV to 1.53 eV. One can then calculate the doping density to be $N_D \sim 4 \times 10^{18}\text{cm}^{-3}$.[32] As shown in Figure 5 the Fermi level splitting in the doped pillars can reach values larger than 1.07 eV under 1 sun illumination intensity, about 0.46 eV below the absorption edge of the material, similar to what was achieved with the surface treated pillars. This value for $E_g - qV_{OC}$ is similar to what has been achieved in the record planar InP solar cell.[14] These results clearly show the benefit of increasing the spontaneous emission rates by doping. While heavy doping can lead to an increase of SRH recombination as it introduces defects, it has been reported that InP materials can be doped very highly without significant losses in the internal quantum yields for spontaneous emission.[33]

Another strategy to increase the brightness of pillars is to improve the light extraction efficiency. This can be realized by random surface texturing.[34] Figure 6a,b shows a flower-shaped nanotextured InP micropillar. The structure was synthesized via a two-step growth process. First, a regular undoped pillar such as shown in Figure 1a was grown. Subsequently, the pillars were overgrown with additional intrinsic InP material at a greatly reduced V/III ratio, resulting in localized, protruding features. TEM studies revealed that the micropillar assumes a single-crystalline wurtzite structure in the core which was grown in the


dx.doi.org/10.1021/nl500621j | Nano Lett. 2014, 14, 3235–3240

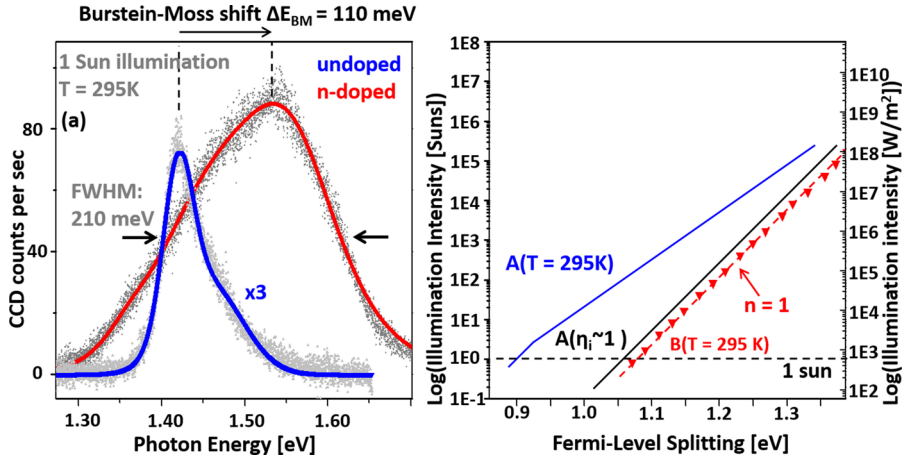


**Figure 5.** (a) Spectra of undoped (blue line) and n-doped (red line) pillars under 1 sun illumination condition. (b) Comparisons of contactless $I-V$ characteristics of undoped micropillar (traces A) and doped micropillar (trace B).

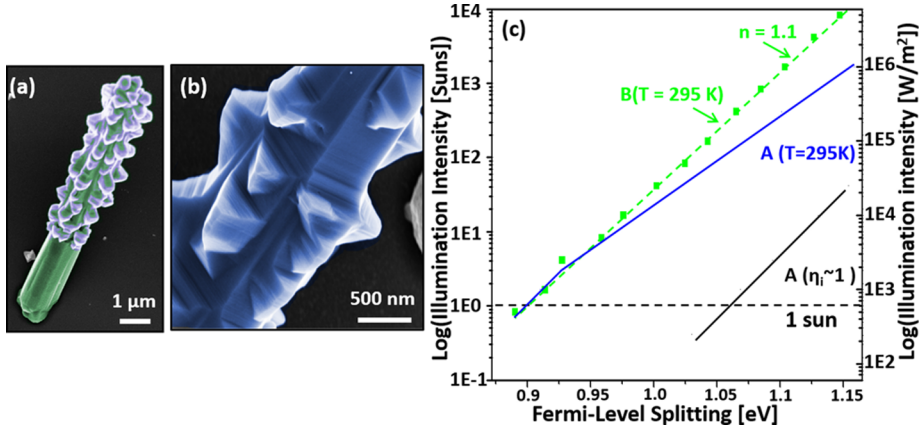


**Figure 6.** (a, b) SEM images of flower-shaped pillar with close-up view shown in (b). (c) Comparisons of contactless $V-I$ characteristics of a regular pillar (traces A) and a flower-shaped pillar (trace B).

first step, while the flower-shaped, protruding features exhibit a high density of stacking faults. The absorptivity of such pillars can be estimated to be ~2 (see Supporting Information). As seen in Figure 6c, the Fermi level splitting obtained from a flower-shaped micropillar (trace B in Figure 6c) is at 0.90 eV at 1 sun, which is similar compared to what is found in undoped regular pillars (compare with trace A in Figure 6c). This result is remarkable given the high density of stacking faults, showing the effectiveness of nanotextured surfaces for enhancing light extraction efficiencies.

In conclusion, a contactless technique was utilized to assess the potential of InP micropillars for photovoltaic applications. Several strategies for enhancing the external quantum yield for spontaneous emission, which is intimately related to Fermi level splitting, were studied. Chemical removal of the native oxide yielded splitting of ~0.95 eV, which is 0.47 eV below the bandgap and a significant improvement compared to the free energy loss of 0.52 eV found in untreated pillars. Inclusion of nanotextures on pillar surfaces can enhance the light extraction efficiencies. It was found that textured pillars with high densities of stacking faults can still achieve similar Fermi splitting as regular pillars with high crystal quality. Unfortunately, the fabrication of nanotextures without the introduction of defects is an inherently difficult problem. In our studies doping of the material proved to be the most effective approach, showing that $\Delta F \sim 1.071$ eV could be obtained in InP micropillars, 0.46 eV below the absorption band edge of the material. This value for $E_g - qV_{OC}$ is the lowest for InP grown on a silicon substrate and at par with what has been achieved in the record planar InP solar cell on an InP substrate.[14]

The results presented here confirm that InP micropillar materials have the potential of achieving high open-circuit voltages; such structures could be grown on lattice mismatched substrates such as silicon which could be low-cost, especially if low-grade silicon or polysilicon were to be used.[35] Since in this instance the substrates do not serve as the light absorbers material there are no strict requirements on the substrate materials quality as long as the substrate can be doped sufficiently high enough such that losses due to electrical resistances are low.

## ■ ASSOCIATED CONTENT

### Supporting Information

Impact of free energy loss on solar cell efficiencies; calibration of collection efficiency of photoluminescence setup; angle-averaged absorptivity of InP micropillars; calculated Fermi level splitting as a function of photon energy; estimation of the error of the Fermi level splitting. This material is available free of charge via the Internet at http://pubs.acs.org.


dx.doi.org/10.1021/nl500621j | Nano Lett. 2014, 14, 3235−3240

## AUTHOR INFORMATION


### Corresponding Author

*E-mail cch@berkeley.edu (C.J.C.-H.).


### Notes

The authors declare no competing financial interest.

## ACKNOWLEDGMENTS

This work was supported by the U.S. DOE SunShot Program via Contract DE-EE0005316, DoD NSSEFF Fellowship via Contracts N00244-09-1-0013 and N00244-09-1-0080, and the California Advanced Solar Technologies Institute, UC Multi-campus Research Program and Initiatives (MRPI). The authors acknowledge the support of the National Center for Electron Microscopy, Lawrence Berkeley Laboratory, for the use of their facilities.

## REFERENCES


(1) Wang, X.; Kurdgelashvili, L.; Byrne, J.; Barnett, A. *Renewable Sustainable Energy Rev.* **2011**, *15*, 4248−4254.

(2) Yablonovitch, E.; Gmitter, T.; Harbison, J. P.; Bhat, R. *Appl. Phys. Lett.* **1987**, *51*, 2222−2224.

(3) Martensson, T.; Svensson, C. P. T.; Wacaser, B. A.; Larsson, M. W.; Seifert, W.; Deppert, K.; Gustafsson, A.; Wallenberg, L. R.; Samuelson, L. *Nano Lett.* **2004**, *4*, 1987−1990.

(4) Heurlin, M.; Wickert, P.; Falt, S.; Borgstrom, M. T.; Deppert, K.; Samuelson, L.; Magnusson, M. H. *Nano Lett.* **2011**, *11*, 2028−2031.

(5) Holm, V.; Jørgensen, H. I.; Krogstrup, P.; Nygård, J.; Liu, H.; Aagesen, M. *Nat. Commun.* **2013**, *4*, 1498.

(6) Krogstrup, P.; Jørgensen, H. I.; Heiss, M.; Demichel, O.; Holm, J. V.; Aagesen, M.; Nygard, J.; Fontcuberta i Morral, A. *Nat. Photonics* **2013**, *7*, 306−310.

(7) Yoshimura, M.; Nakai, E.; Tomioka, K.; Fukui, T. *Appl. Phys. Express* **2013**, *6*, 052301.

(8) Mariani, G.; Scofield, A. C.; Hung, C.-H.; Huffaker, D. L. *Nat. Commun.* **2013**, *4*, 1497.

(9) Wallentin, J.; Anttu, N.; Asoli, D.; Huffman, M.; Aberg, I.; Magnusson, M.; Siefer, G.; Fuss-Kailuweit, P.; Dimroth, F.; Witzigmann, B.; Xu, H. Q.; Samuelson, L.; Deppert, K.; Borgstrom, M. T. *Science* **2013**, *339*, 1057−1060.

(10) Cui, Y.; Wang, J.; Plissard, S. R.; Cavalli, A.; Vu, T. T. T.; van Veldhoven, R. P. J.; Gao, L.; Trainor, M.; Verheijen, M. A.; Haverkort, J. E. M.; Bakkers, E. P. A. M. *Nano Lett.* **2013**, *13*, 4113−4117.

(11) LaPierre, R. R.; Chia, A. C. E.; Gibson, S. J.; Haapamaki, C. M.; Boulanger, J.; Yee, R.; Kuyanov, P.; Zhang, J.; Tajik, N.; Jewell, N.; Rahman, K. M. A. *Phys. Status Solidi RRL* **2013**, *10*, 815−830.

(12) Ross, R. T. J. *Chem. Phys.* **1967**, *46*, 4590−4593.

(13) Miller, O. D.; Yablonovitch, E.; Kurz, S. R. http://arxiv.org/abs/1106.1603, 2012.

(14) Green, M. A.; Emery, K.; Hishikawa, Y.; Warta, W.; Dunlop, E. D. *Prog. Photovoltaics* **2013**, *21*, 827−837.

(15) Cirlin, G. E.; Bouravleuv, A. D.; Soshnikov, I. P.; Samsonenko, Y. B.; Dubrovskii, V. G.; Arakcheeva, E. M.; Tanklevskaya, E. M.; Werner, P. *Nanoscale Res. Lett.* **2010**, *5*, 360−363.

(16) Tajik, N.; Peng, Z.; Kuyanov, P.; LaPierre, R. R. *Nanotechnology* **2011**, *22*, 225402.

(17) Cho, K.; Ruebusch, D. J.; Lee, M. H.; Moon, J. H.; Ford, A. C.; Kapadia, R.; Takei, K.; Ergen, O.; Javey, A. *Appl. Phys. Lett.* **2011**, *98*, 203101.

(18) Wurfel, P. *J. Phys. C* **1985**, *15*, 3967−3985.

(19) Trupke, T.; Bardos, R. A.; Schubert, M. C.; Warta, W. *Appl. Phys. Lett.* **2006**, *89*, 044107.

(20) Delamarre, A.; Lombez, L.; Guillemoles, J. F. *Appl. Phys. Lett.* **2012**, *100*, 131108.

(21) Casey, H. C., Jr.; Buehler, E. *Appl. Phys. Lett.* **1977**, *30*, 247−249.

(22) Ren, F.; Ng, K. W.; Li, K.; Sun, H.; Chang-Hasnain, C. J. *Appl. Phys. Lett.* **2013**, *102*, 012115.

(23) Ng, K. W.; Ko, W. S.; Tran, T.-T. D.; Chen, R.; Nazarenko, M. V.; Lu, F.; Dubrivskii, V. G.; Kamp, M.; Forchel, A.; Chang-Hasnain, C. J. *ACS Nano* **2013**, *7*, 100−107.

(24) Mattila, M.; Hakkarainen, T.; Mulot, M.; Lipsanen, H. *Nanotechnology* **2006**, *17*, 1580−1583.

(25) Li, K.; Tran, T.; Ng, K. W.; Sun, H. Lu, F. L.; Chang-Hasnain, C. J. In 55th Electronic Materials Conference, South Bend, IN, June 26−28, 2013.

(26) Breuer, S.; Pfuller, C.; Flissikowski, T.; Brandt, O.; Grahn, H. T.; Geelhaar, L.; Riechert, H. *Nano Lett.* **2011**, *11*, 1276−1279.

(27) Jiang, N.; Parkinson, P.; Gao, Q.; Breuer, S.; Tan, H. H.; Wong-Leung, J.; Jagadish, C. *Appl. Phys. Lett.* **2012**, *101*, 023111.

(28) Chuang, S. L. *Physics of Optoelectronic Devices*, 1st ed.; Wiley: New York, 1995; Chapter 10.

(29) Miller, R. C.; Kleinman, D. A.; Nordland, W. A., Jr.; Gossard, A. C. *Phys. Rev. B* **1980**, *22*, 863−871.

(30) Schmidt, T. M. *Appl. Phys. Lett.* **2006**, *89*, 123117.

(31) Sun, Y.; Liu, Z.; Machuca, F.; Pianetta, P.; Spicer, W. E. J. *Appl. Phys.* **2005**, *97*, 124902.

(32) Liu, C.; Dai, L.; You, L. P.; Xu, W. J.; Qin, G. G. *Nanotechnology* **2008**, *19*, 465203.

(33) Luryi, S.; Subashiev, A. V. *Nucl. Instrum. Methods Phys. Res., Sect. A* **2011**, *652*, 292−294.

(34) Boroditsky, M.; Ragan, R.; Yablonovitch, E. *Sol. Energy Mater. Sol. Cells* **1999**, *57*, 1−7.

(35) Ng, K. W.; Ko, W.; Chen, R.; Tran, T.; Lu, F.; Chuang, L. C.; Sedwick, F. G.; Chang-Hasnain, C. In IEEE Photonics Society, 23rd Annual Meeting, Denver, CO, Nov 7−11, 2010.